Journal of Materials Chemistry A

PAPER

View Article Online
View Journal | View Issue

Cite this: J. Mater. Chem. A, 2015, 3, 12858

Received 30th April 2015
Accepted 18th May 2015

DOI: 10.1039/c5ta03196f

www.rsc.org/MaterialsA

Ionic conductivity of a single porous MnO_2 mesorod at controlled oxidation states†

Timothy Plett,[a] Trevor Gamble,[a] Eleanor Gillette,[b] Sang Bok Lee[b] and Zuzanna S. Siwy*[ac]

The ionic conductivity of porous MnO_2 at the nanoscale is not well understood, despite possible importance in battery charging/discharging processes. It is demonstrated here that MnO_2 in different oxidation states exhibits different ionic conductivities and surface charge characteristics, which are probed by reversal potential measurements.

Introduction

Nanopores have been leveraged for use as templates in fabricating nanowire arrays by electrodeposition.[1] A wide spectrum of materials can be electrodeposited, including metals,[2] metal oxides,[3] and polymers,[3] as well as composite structures such as PEDOT/MnO_2 coaxial structures.[4] The main use for this technique has been to deposit a desired material in the nanopore template, then etch away the membrane to access the wires. However, there are cases where removal of the template is not needed. For example, the template can serve as a separator in fully integrated nanobatteries.[5] The template can also be used to confine materials to the nanoscale, to investigate their ionic transport properties and geometry, as we demonstrated for MnO_2 mesorods previously.[6]

MnO_2 is a popular material for energy storage devices, due to its high theoretical capacitance and low cost. When electrodeposited, it has a porous structure as recently revealed by microscopy and electrochemical measurements.[6] MnO_2 has come under investigation in recent years due to the discovery of its supercapacitor nature at the nanoscale.[7] This has generated electrode designs that rely on densely packed nanostructures, utilizing conductive additives or scaffolds to boost electrical conductivity, and thus improve power density.[8] However, power is not just limited by electric conductivity, but also by ionic access in these porous, densely packed structures. In order to optimize ionic conductivity in the MnO_2 nanovoids, methods are needed to quantify it, and to understand how the conductivity may change during charging and discharging.

Here we use the template method to electrodeposit a single MnO_2 mesorod in a single-pore polymer membrane. In contrast to our previous study,[6] the MnO_2 in this case is not a static plug, but serves as a model nanoscale electrode. It is connected to an external circuit so that its oxidation state can be electrochemically altered while ionic conductivity measurements are taking place. The recorded ion currents reflect ionic transport through the porous structure of the material, thus they are de-coupled from the electronic transport. This method provides a unique platform for understanding how structural and electrochemical changes could influence ion access to active material during the charging and discharging of a supercapacitor.

Experimental methods

Template preparation

Single pore templates were prepared by the track-etching technique, in which 12 μm thick polyethylene terephtalate films were irradiated with single, energetic heavy ions, followed by wet chemical etching.[9] The irradiation was performed at the Institute for Heavy Ions Research in Darmstadt, Germany. The irradiated foils were etched in 0.5 M NaOH, 70 °C. Pore opening diameter increases linearly with time, and 30 min of etching in these conditions enlarges the pore by ~100 nm.[10] Opening diameter of single pores was subsequently measured by recording current–voltage curves of the pores in 1 M KCl, pH 8, as described before.[11] ESI† presents a scheme of a conductivity cell used in the measurements. The obtained pore resistance was used to calculate an effective pore opening diameter. The template pores used in this study had diameter between 150 and 350 nm.

MnO_2 deposition

In order to create external electrical contact, one side of the membrane was sputtered with ~50 nm of gold. It was confirmed that the gold layer did not cover the single nanopores and they

[a]Department of Physics, University of California, Irvine, Irvine, CA 92697-4575, USA. Fax: +1 9498242174; Tel: +1 9498246911. E-mail: zsiwy@uci.edu

[b]Department of Chemistry and Biochemistry, University of Maryland, College Park, Maryland 20742, USA. Fax: +1 3013149121; Tel: +1 3013149121

[c]Department of Chemistry, University of California, Irvine, Irvine, CA 92697-2025, USA. Fax: +1 9498248571; Tel: +1 9498244097

† Electronic supplementary information (ESI) available: Full derivation of particles scattering into a cylinder, experimental apparatus, multipore SEM, MnO_2 reversibility data, and *I–V* Curves also given. See DOI: 10.1039/c5ta03196f

could still pass ionic current (ESI†). The open character of the pore is the main difference between the previous study[6] and this experiment. The gold layer became an integral part of the device, facilitating the electrodeposition of MnO_2 and changing its oxidation state. MnO_2 deposition was performed from 100 mM manganese acetate solution at 0.6 V *vs.* Ag/AgCl.[6]

Experimental procedure

Ionic conductivity and reversal potential experiments were performed on the MnO_2 mesorods in a two-probe measurement, utilizing a Keithley 6487 Picoammeter. After each set of conductivity measurements, the MnO_2 sample would be lithiated or delithiated in cell by a CH Instruments 650C Electrochemical Analyzer. The reference electrode used was Ag/AgCl (3 M) and a Pt wire was used as a counter electrode for the system. Fig. 1a and b depict the experimental set up for each procedure.

Results and discussion

The process of preparation of a single MnO_2 rod, which could be electrically addressed, started with sputtering one side of the single pore membranes with Au. Based on earlier studies,[12] a gold layer at least 10 nm thick can serve as an electrode. In order to predict the working depth of the gold layer, sputter deposition was considered as a homogeneous scattering of point particles in three-dimensions. Then, an approximation for the thickness of gold inside a nanopore, λ_d, at a certain depth, d, based on the pore radius, r, and the gold thickness at the surface, λ_0 was obtained (see ESI†):

$$\lambda_d = \lambda_0 \frac{\Delta}{\pi} \sum_{\theta_z=0}^{\theta_{z\,max}} 2\tan^{-1}\left(\frac{\sqrt{(2r - d\tan(\theta_z))d\tan(\theta_z)}\cos(\theta_z)}{d}\right) \Big/ \pi \quad (1)$$

$$\theta_{z\,max} = \arctan\left(\frac{2r}{d}\right)$$

Fig. 2 models the thickness ratio between the gold layer on the surface of the membrane, λ_0, and λ_d, as a function of depth, d. This is calculated for three scattering conditions above the pore, where the azimuthal angle through which Au particles may scatter is varied: full hemisphere scattering (π), restricted hemisphere scattering ($2\pi/3$), and reduced hemisphere scattering ($\pi/2$). For a 50 nm thick sputtered layer of gold, and a 200 nm opening diameter pore, we expect the working distance for the gold layer to extend ~50 nm to 100 nm into the pore.

This gold layer provided a contact to electrodeposit MnO_2 inside the pore. The same electrodeposition procedure was used as reported before,[6] namely 100 mM manganese acetate solution at 0.6 V *vs.* Ag/AgCl, which leads to the following electrochemical reaction:

$$Mn^{2+} + 2H_2O \rightarrow MnO_2 + 4H^+ + 2e^- \quad (2)$$

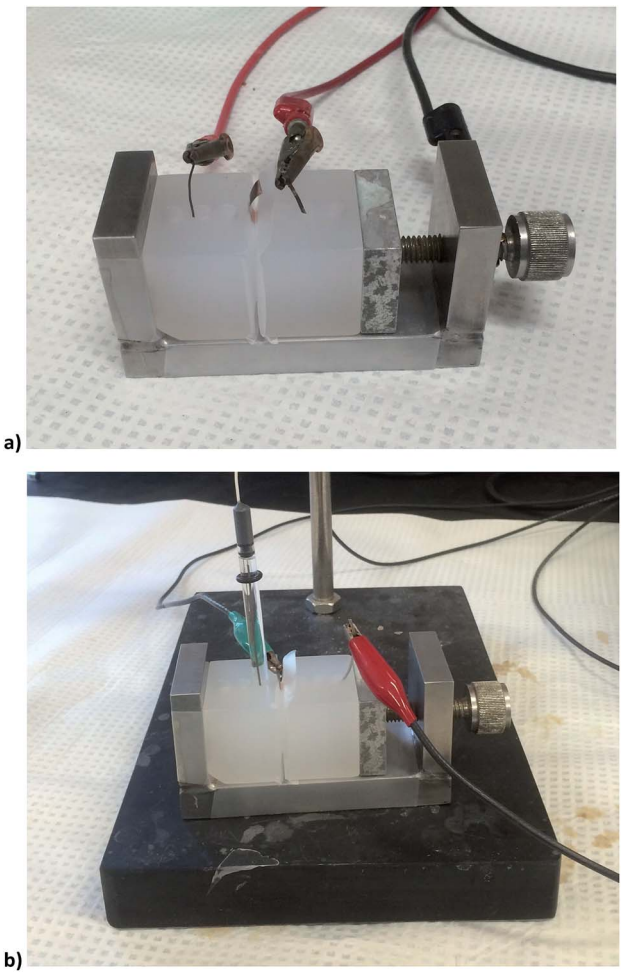

Fig. 1 (a) Picture of the two-probe measurement for a standard conductivity measurement. (b) The three-probe set up for the lithiation and delithiation procedure (Working – green; Counter – red).

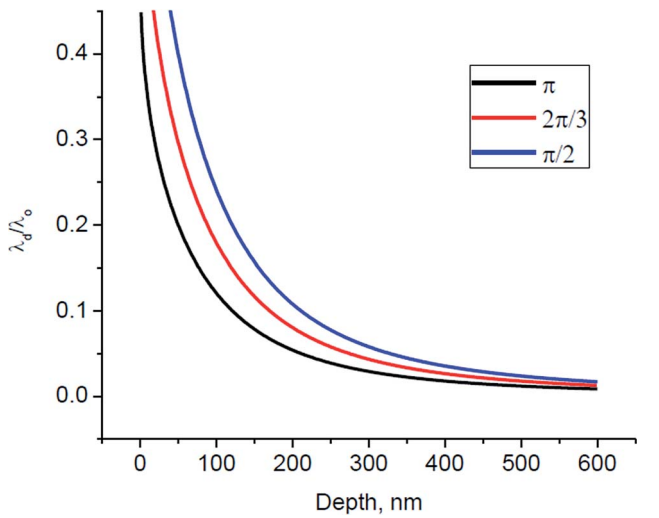

Fig. 2 Numerical solutions to eqn (1) expressed as a ratio of gold thickness at a given depth, λ_d, and gold thickness on the surface, λ_0. Three scattering conditions are considered. In case of the full hemisphere scattering (π) for a 200 nm diameter pore, a 50 nm thick surface layer is attenuated to 10 nm thickness at $d \sim 60$ nm.

Successful formation of a MnO_2 rod was confirmed using two types of measurements. (i) First, we compared the ionic conductivity of a single pore before and after deposition of MnO_2. Similar to the previous report,[6] the presence of a rod significantly increased the system resistance, as shown in Fig. 3 for a ~1 μm long rod deposited in a 325 nm diameter pore. This measurement also confirms the deposited rod creates a mesh with connected voids, so that the system still exhibits finite conductance.[6] The samples demonstrated less dramatic changes in resistance than observed previously, possibly due to the effect of the gold electrode on the pore wall. The single pore/rod samples prepared for this study often featured ion current rectification, such that positive currents were higher than negative currents. Positive voltage in our electrode configuration indicates the anode located at the side of the membrane with deposited MnO_2 thus higher currents correspond to cations moving from the MnO_2 mesh to the open side of the template pore. The asymmetric current–voltage curves can be attributed to the negative surface charge of the MnO_2 (ref. 6) and its nanometer-scale voids. The extended, micrometer length of the mesorod compared to the previous study (200 nm) also favours rectification. As shown recently, rectification of ion current in nanopores and nanovoids requires a certain minimum length of the pore with ionic selectivity characteristics.[13] The rectification of the examined MnO_2 rods can be compared to conically shaped nanopores,[14] which also demonstrate preference in transporting cations from the small opening to the base of the cone.

(ii) The second measurement which confirmed successful deposition of single rods involved recording current–voltage curves for a wide set of KCl concentrations. For porous structures which carry excess surface charges on the pore walls, a saturation of ion current is observed such that further lowering of a bulk electrolyte concentration does not change the magnitude of the measured current.[15,16] The currents start to saturate at conditions at which the pore radius approaches the thickness of the electrical double-layer. Similar to the study by Gamble *et al.*,[6] ion current saturation was again observed in the samples prepared for this report. For the mesorod shown in Fig. 4a and b the KCl concentration at which saturation occurred was ~10 mM, which suggests the voids have opening of ~3 to 6 nm.

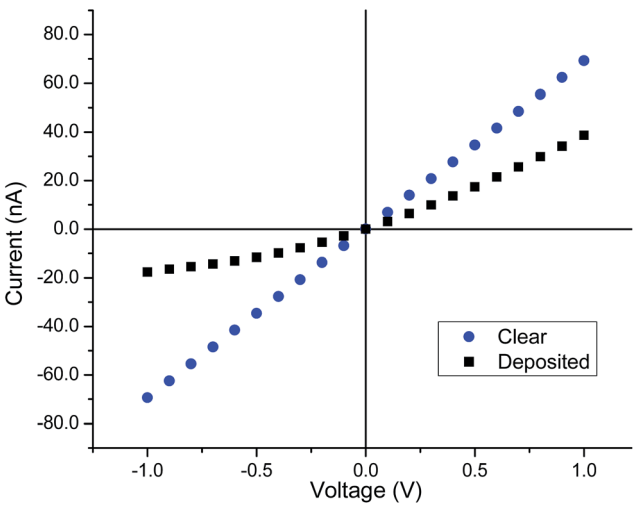

Fig. 3 *I–V* curves showing the difference in a 325 nm pore after MnO_2 deposition, as well as the resulting rectification behaviour.

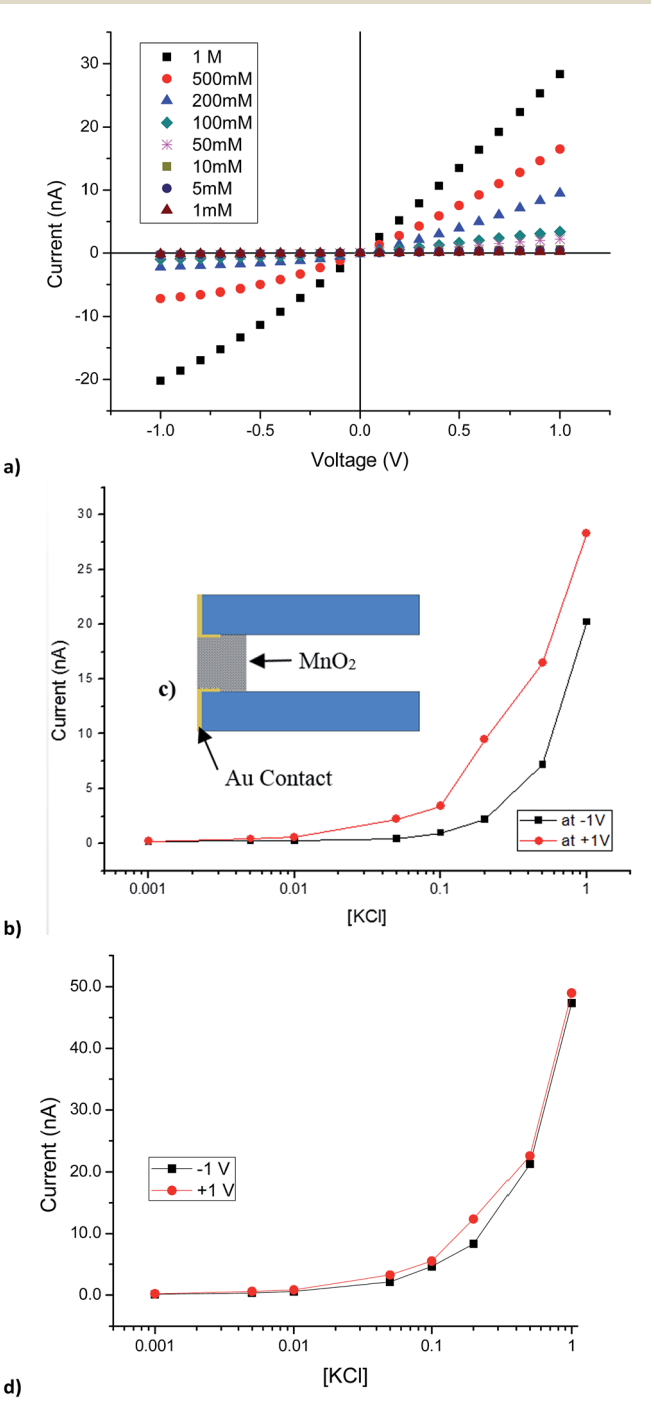

Fig. 4 (a) *I–V* curves and (b) semi-log plot of current *vs.* concentration of a single MnO_2 mesorod deposited in a 250 nm in diameter pore. Saturation of ion current with bulk electrolyte (KCl) concentration occurs at ~10 mM. Inset (c) is a representation of the pore-rod system. (d) Ion current saturation in lithiated MnO_2 rod demonstrates presence of surface charge and no significant changes to void size.

Finally, successful electrodeposition of mesorods in the pores using the 50 nm gold sputtered film was also demonstrated with commercial multipore polymer membranes. We used Whatman 200 nm multipore (10^8 cm^{-2}) polycarbonate membranes. SEM images of MnO_2 mesorods and *I–V* curves can be found in the ESI.†

After performing *I–V* curves for the newly deposited single wires, some samples were selected for lithium insertion and discharge according to the equation:

$$MnO_2 + xLi^+ + xe^- \leftrightarrow Li_x(Mn_x^{3+}Mn_{1-x}^{4+})O_2 \quad (3)$$

Insertion was carried out in non-aqueous (propylene carbonate) 100 mM $LiClO_4$ solution at −0.22 V *vs.* Ag/AgCl, a voltage which has been reported to produce a Li : Mn ratio of 1.0.[17] Ion currents were tested for clear, deposited, 'lithiated', and 'delithiated' states of the samples in aqueous KCl solutions ranging from 1 M to 1 mM. KCl was the salt of choice due to nearly equal mobilities of the two ions. Fig. 5a shows *I–V* curves for a 325 nm diameter mesorod in three states: deposited, lithiated, and delithiated.

The change of the pore resistance is summarized in the form of bar graphs in Fig. 5b with currents for positive and negative voltages respectively. Lithiation of the rod causes a decrease of positive current and increase of negative current. This curtailing of rectification suggests a reduction of the excess negative charge on MnO_2. Subsequent discharge increases current for positive voltage polarity and increases the rectification effect. Similar behavior was found with two independently prepared MnO_2 mesorods subjected to two cycles of lithiation/delithiation. Fig. 5c summarizes recordings obtained with a mesorod deposited in a single pore with an opening diameter of 240 nm.

In order to further probe the lithiation-induced changes in observed ionic conductance, surface charge on the MnO_2 rod at the lithiated state was also probed by measuring current voltage curves in a wide range of KCl concentrations. Similar to the as-deposited rods, currents through lithiated MnO_2 exhibited saturation at ~10 mM (see Fig. 4d); the measurements therefore indicate that the lithiated MnO_2 still carries negative surface charge on the voids, as suggested by the residual rectification properties shown in Fig. 5. A similar character of the saturation curves before and after lithiation allows us to conclude that the effective size of the voids in the material is not significantly affected by lithiation. More detailed description of surface charge at different oxidation states was probed by the so-called reversal potential measurements. Reversal potential, V_{rev}, indicates the magnitude of a potential difference that develops across an ion selective membrane that is in contact with a salt concentration gradient. At room temperature, a 10-fold difference in ionic concentrations on both sides of a perfectly anion or cation selective membrane develops reversal potential equal to a Nernst potential of ~59 mV. This is detected as an *I–V* curve not passing through the origin of the coordinate system, but rather being shifted to the right or left (depending on salt configuration as well as on anionic or cationic

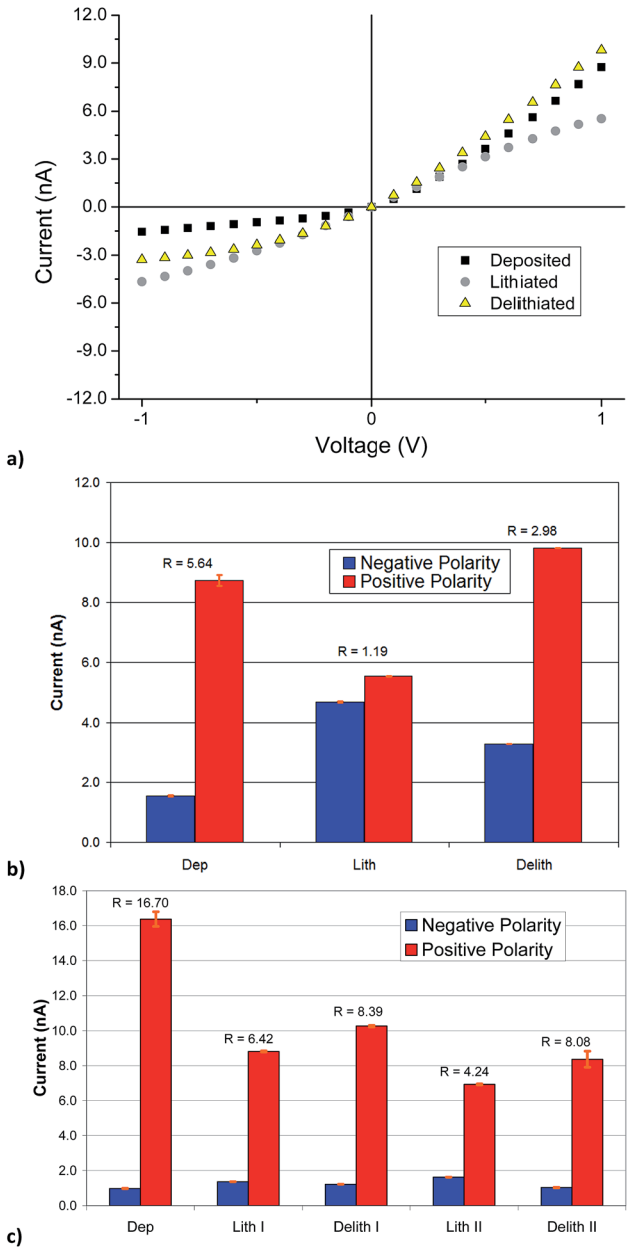

Fig. 5 (a) Averaged *I–V* curves for forward and reverse scans of a MnO_2 rod at lithiated and delithiated states. (b) Histograms of ionic current at ±1 V show the change in rectification factor, which is calculated: $R = I(+1\text{ V})/I(-1\text{ V})$. (c) Summary of ionic current in a 240 nm pore, demonstrating cyclability.

selectivity) by 59 mV. If there is no selectivity, the *I–V* curve goes through zero. If a membrane is partially selective, the shift occurs between 0 and 59 mV. A general description of ionic selectivity is provided by the Goldman–Hodgkin–Katz eqn (4) which links the magnitude of the reversal potential with a ratio of effective diffusion coefficients of both ions in the pore, x:[18]

$$V_{rev} = \frac{RT}{F}\ln\frac{x[K^+]_1 + [Cl^-]_2}{x[K^+]_2 + [Cl^-]_1} \quad \text{where } x = \frac{D^K_{pore}}{D^{Cl}_{pore}} \quad (4)$$

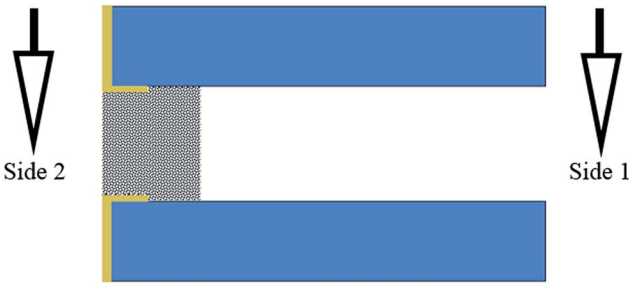

Fig. 6 Schematic of reversal potential measurement set-up.

The subscripts in the equation represent the different sides of the MnO_2 rod. Fig. 6 gives a simple schematic for our experiment. For the entirety of our experiment, the MnO_2 rod and the working electrode are on side 2 of the membrane. Therefore, a positive V_{rev} for a concentration arrangement of 0.1 M (side 1) and 10 mM (side 2) indicates cation selectivity. Inversely, a negative V_{rev} for a concentration distribution of 10 mM (side 1) and 0.1 M (side 2) also indicates cation selectivity. Selectivity of a 250 nm diameter MnO_2 mesorod was probed using two electrolyte configurations: 0.1 M/10 mM and 10 mM/0.1 M (Table 1). Measurements for the initial deposition confirm the negative surface charge and cation selectivity (for 0.1 M (1)/0.01 M (2), eqn (4) yields $x \sim 7$).

In the 'lithiated' state, the sign of reversal potential measurements suggested MnO_2 still carried negative surface charge; a reduced magnitude of V_{rev} indicates, however, that some of the negative charge in the MnO_2 surface may be reduced by the presence of intercalated lithium. The reduction of V_{rev} is more pronounced in the case when the solution with higher KCl concentration was present on the side of the membrane with the mesorod. The enhanced dependence of the cation selectivity on the salt concentration in contact with the rod might be explained by the lowered overall negative charge on the manganese oxide. Since the excess concentration of counterions in the voids is a function of void diameter and surface charge density of the porous material,[15,16] after lithiation the voids remain selective only at low salt concentrations. This is consistent with previous observations of MnO_2 in a lithium perchlorate solution, which suggest that there is some surface adsorption of lithium even without applied potential.[17] Therefore, significant differentiation of reversal potential between lithiated and delithiated states at these concentrations may not be detectable.

Table 1 Full reversal potential measurements for a 250 nm diameter mesorod as it passes through two charging cycles

S(1)/S(2)	Deposit	Lith I	Delith I	Lith II	Delith II
100/10[a]	+45 mV	+33 mV	+35 mV	+30 mV	+35 mV
10/100	−50 mV	−30 mV	−30 mV	−25 mV	−25 mV

[a] The concentration configurations are given in concentration units of mM and are arranged where S(1) is side 1 and S(2) is side 2, which is the side of the deposited MnO_2 (Fig. 5). The electrode bias remained $<\pm 3$ mV in all reversal potential measurements.

Conclusions

We present a method to probe ionic properties of electrode materials. The measured current reflects the transport through the material probing its porous structure. To the best of our knowledge this is the only experimental set-up which allows measuring ionic properties of the electrodes, being totally separated from electronic properties. These results highlight the effect of oxidation state on the ion transport properties in MnO_2 nanostructures. They also demonstrate the viability of a new device capable of changing the oxidation state of a single mesowire as well as resolving its ion transport properties. Future work is planned to leverage this device in the study of other porous materials capable of ion transport and electrochemical reduction.

Acknowledgements

This work was funded by the Nanostructures for Electrical Energy Storage (NEES), an Energy Frontier Research Center funded by the US Department of Energy, Office of Science, Office of Basic Energy Sciences under Award Number DESC001160. We also acknowledge GSI Helmholtzzentrum für Schwerionenforschung in Darmstadt, Germany for providing irradiated membranes, the Maryland NanoCenter and its NISP Laboratory for the use of SEM, and UCI Calit-2 and its LEXI facility for the use of SEM.

Notes and references

1 (*a*) C. R. Martin, *Science*, 1994, **266**, 1961–1966; (*b*) C. J. Brumlik, V. P. Menon and C. R. Martin, *J. Mater. Res.*, 1994, **9**, 1174–1183.
2 (*a*) C. Schönenberger, *et al.*, *J. Phys. Chem. B*, 1997, **101**, 5497–5505; (*b*) M. E. Toimil-Molares, V. Buschmann, D. Dobrev, R. Neumann, R. Scholz, I. U. Schuchert and J. Vetter, *Adv. Mater.*, 2001, **13**, 62–65; (*c*) T. W. Cornelius, J. Brötz, N. Chtanko, D. Dobrev, G. Miehe, R. Neumann and M. E. Toimil Molares, *Nanotechnology*, 2005, **16**, S246–S249.
3 *Nanostructured Materials in Electrochemistry*, ed. A. Eftekhari, Wiley-VCH, Weinheim, 2008.
4 J. Duay, E. Gillette, R. Liu and S. B. Lee, *Phys. Chem. Chem. Phys.*, 2012, **14**, 3329–3337.
5 C. Liu, *et al.*, *Nat. Nanotechnol.*, 2014, **9**, 1031–1039.
6 T. Gamble, E. Gillette, S. B. Lee and Z. S. Siwy, *J. Phys. Chem. C*, 2013, **117**, 24836–24842.
7 H. Y. Lee and J. B. Goodenough, *J. Solid State Chem.*, 1999, **144**, 220–223.
8 S. Santhanagopalan, A. Balram and D. D. Meng, *ACS Nano*, 2013, **7**(3), 2114–2125.
9 (*a*) R. L. Fleischer, P. B. Price and R. M. Walker, *Nuclear Tracks in Solids: Principles and Applications*, University of California Press, Berkeley CA, 1975; (*b*) R. Spohr, German Patent DE 2951376 C2, 1983trans*US Pat.* 4369370, 1983.
10 M. Pevarnik, K. Healy, K. M. E. Toimil-Molares, A. Morrison, S. E. Letant and Z. S. Siwy, *ACS Nano*, 2012, **6**, 7295–7302.

11 P. Yu. Apel, Y. E. Korchev, Z. Siwy, R. Spohr and M. Yoshida, *Nucl. Instrum. Methods Phys. Res., Sect. B*, 2011, **184**, 337–346.
12 S.-Y. Kishioka, J. Nishino and H. Sakaguchi, *Anal. Chem.*, 2007, **79**, 6851–6856.
13 J.-F. Pietschmann, *et al.*, *Phys. Chem. Chem. Phys.*, 2013, **15**, 16917–16926.
14 (*a*) Z. S. Siwy, *Adv. Funct. Mater.*, 2006, **16**, 735–746; (*b*) Z. S. Siwy and S. Howorka, *Chem. Soc. Rev.*, 2010, **39**, 1115–1132; (*c*) C. Wei, A. J. Bard and S. W. Feldberg, *Anal. Chem.*, 1997, **69**, 4627–4633.
15 D. Stein, M. Kruithof and C. Dekker, *Phys. Rev. Lett.*, 2004, **93**, 035901.
16 R. B. Schoch, J. Han and P. Renaud, *Rev. Mod. Phys.*, 2008, **80**, 839–883.
17 J. Song, J. Duay, E. Gillette and S. B. Lee, *Chem. Commun.*, 2014, **50**, 7352–7355.
18 B. Hille, *Ion Channels of Excitable Membranes*, Sinauer Associates, Sunderland, MA, 3rd edn, 2001.